



RESEARCH LETTER

10.1002/2015GL064772

Key Points:

- Statistical analysis of natural versus induced seismicity, preproduction, and coproduction
- Both have same frequency-size, interevent time, and spatial distribution statistics
- Nearest neighbors derived from space-time-magnitude reveal statistical differences of clustering

Supporting Information:

- Figures S1–S7

Correspondence to:

M. Schoenball,
mschoenball@usgs.gov

Citation:

Schoenball, M., N. C. Davatzes, and J. M. G. Glen (2015), Differentiating induced and natural seismicity using space-time-magnitude statistics applied to the Coso Geothermal field, *Geophys. Res. Lett.*, 42, 6221–6228, doi:10.1002/2015GL064772.

Received 2 JUN 2015

Accepted 10 JUL 2015

Accepted article online 15 JUL 2015

Published online 3 AUG 2015

Differentiating induced and natural seismicity using space-time-magnitude statistics applied to the Coso Geothermal field

Martin Schoenball^{1,2}, Nicholas C. Davatzes¹, and Jonathan M. G. Glen²

¹Earth and Environmental Science, Temple University, Philadelphia, Pennsylvania, USA, ²GMEG Science Center, U.S. Geological Survey, Menlo Park, California, USA

Abstract A remarkable characteristic of earthquakes is their clustering in time and space, displaying their self-similarity. It remains to be tested if natural and induced earthquakes share the same behavior. We study natural and induced earthquakes comparatively in the same tectonic setting at the Coso Geothermal Field. Covering the preproduction and coproduction periods from 1981 to 2013, we analyze interevent times, spatial dimension, and frequency-size distributions for natural and induced earthquakes. Individually, these distributions are statistically indistinguishable. Determining the distribution of nearest neighbor distances in a combined space-time-magnitude metric, lets us identify clear differences between both kinds of seismicity. Compared to natural earthquakes, induced earthquakes feature a larger population of background seismicity and nearest neighbors at large magnitude rescaled times and small magnitude rescaled distances. Local stress perturbations induced by field operations appear to be strong enough to drive local faults through several seismic cycles and reactivate them after time periods on the order of a year.

1. Introduction

A growing number of confirmed cases of seismicity induced through human activities [Ellsworth, 2013; Grünthal, 2014; Zang *et al.*, 2014] have created a strong demand to recognize induced seismicity, to characterize it, and to find methods to distinguish it from natural seismicity. Analyzing scaling relations and clustering of natural earthquakes has provided us with important insights into the processes that drive seismicity such as tectonic loading, static and dynamic stress changes, fluid flow, and other mechanisms [Kanamori and Brodsky, 2004; Ben-Zion, 2008]. A fundamental unresolved question is whether populations of induced earthquakes share the same scaling relationships as natural earthquakes. Answering this question would tell us to what extent the well-characterized perturbation driving induced seismicity could provide new insights into natural earthquake processes and their relationship to crustal permeability.

The Coso Geothermal Field (CGF) has an abundance of both natural and induced seismicity, with natural seismicity arising from tectonic and magmatic sources [Manley and Bacon, 2000; Hauksson and Unruh, 2007] and induced seismicity arising from geothermal power production [Kaven *et al.*, 2014; Schoenball *et al.*, 2015]. The relevant mechanisms for the observed induced seismicity are net fluid production leading to compaction and subsidence [Fialko and Simons, 2000], pressure increase at reinjection wells, and thermal drawdown.

Here we perform a comparative analysis of natural and induced seismicity using scaling relations of earthquake magnitude, interevent distance, interevent times, and of nearest neighbors pairs defined by a space-time-magnitude distance [Baiesi and Paczuski, 2004; Zaliapin *et al.*, 2008]. We show that natural and induced seismicity are statistically distinct under a combined space-time-magnitude metric defining nearest neighbors, whereas the individual constituents of this metric alone do not have discriminatory power.

2. Field History and Data

Exploration at the CGF began in the 1970s and the first exploration well was spudded in 1977. Four geothermal power plants went online between mid-1987 and 1990 providing 270 MW installed capacity [Monastero, 2002]. Production and injection peaked in the early 1990s and has slowly declined since (Figure 1a).

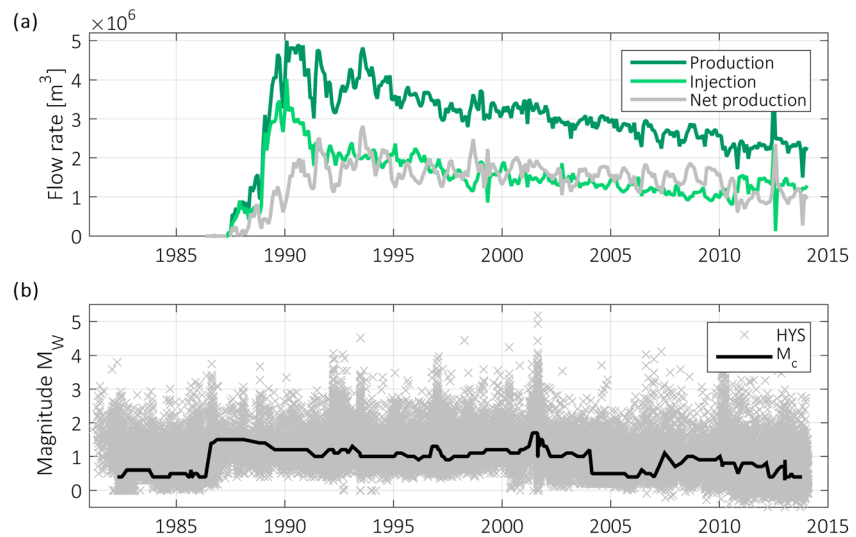


Figure 1. (a) Monthly production, injection, and net production volumes cumulated for the whole field and (b) seismicity and time-varying M_c for 1981–2013.

Two base-line microseismic surveys were conducted within the CGF in summer 1974 and from September 1975 to September 1977 [Combs and Rotstein, 1975; Walter and Weaver, 1980]. Both studies documented a high level of local seismicity. The CGF and surrounding area is among the most seismically active areas in southern California. The largest events within the produced part of the CGF itself are smaller at M4.1 (Figure 1b). Besides the developed portion of the geothermal field, the northwestern part of the CGF has the highest seismic activity throughout the study period from 1981 to 2013 (Figure 2). The largest event to occur during the study period was a magnitude M5.1 earthquake during the July 2001 seismic swarm that occurred along a north-south oriented plane about 6 km west of the produced geothermal field (Figure 2).

In our analysis we consider two study areas. Study area A is defined by $\{35.90^\circ < \text{latitude} < 36.15^\circ; -117.95^\circ < \text{longitude} < -117.65^\circ\}$ and centered on the geothermal field (Figure 2). Study area B is a subregion at the center of A that corresponds to the developed part of the geothermal field defined by $\{35.99^\circ < \text{latitude} < 36.05^\circ; -117.825^\circ < \text{longitude} < -117.760^\circ\}$. Study area A–B is derived as the area inside of A but outside of B.

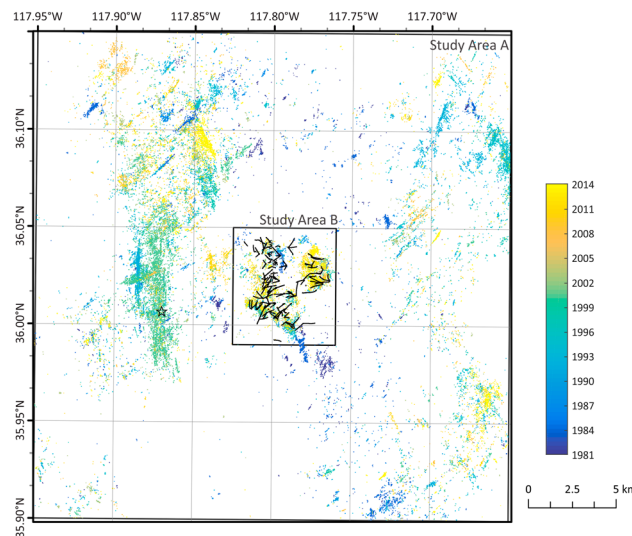


Figure 2. Relocated seismicity around the Coso Geothermal Field from 1981 to 2013 as contained in the HYS catalog. Coloring corresponds to time with younger seismicity projected on top of older seismicity. Wellbore trajectories are shown as black lines. The 2001 M5 event is marked by the star.

We use the HYS catalog [Hauksson et al., 2012] of relocated seismicity in southern California between late 1981 and 2013. It provides precise relative locations using cross correlation in a consistent coverage of study area A (Figure S1 in the supporting information). Due to the large time span of the catalog, the configuration of the seismic network has varied (Figure S2) resulting in corresponding variation of the magnitude of completeness [Hutton et al., 2010]. To estimate the time-dependent magnitude of completeness, M_c , we used the maximum curvature method [Woessner and Wiemer, 2005] applied within a moving window. Windows were 1000 events wide and were moved in 250

events steps through the whole catalog of study area A. This analysis reveals that early parts of the catalog covering the preproduction period until about 1986 had an excellent coverage with $M_c \approx 0.5$. From 1986 to 2004, M_c increased to ~ 1.1 with periods where it increased as high as 1.8. Subsequently, M_c was again ~ 0.5 (Figure 1b). While the maximum curvature method tends to underestimate M_c under certain circumstances (e.g., for the early part until ~ 1986), we are confident that the magnitude of completeness was never larger than 1.8 (Figure S3), and we adopt this value when considering the full extent of the study period from late 1981 to 2013.

We only retained cross correlation relocated events for our analysis which leaves us with about 35,000 events in study area A–B, and about 8000 in study area B. The absolute location uncertainties are on the order of 1 km with 90% of events having location errors < 2.8 km. The relative location uncertainties are generally two orders of magnitude smaller with 90% of events having relative location errors better than 20 m (Figure S1).

2.1. Extent of Induced Seismicity

Induced seismicity as result of field operations at Coso has been previously discussed [Malin, 1994; Feng and Lees, 1998; Lees, 1998; Julian et al., 2010]. The preproduction microseismic surveys of 1975–1977 and also the preproduction part of the HYS catalog show seismicity in study area B, but it does not stand out as a particularly active region of study area A. However, during the coproduction period study area B strongly stands out as the most active volume. Kaven et al. [2014] performed relocations and joint 3-D tomography of the 1996–2012 seismicity recorded by the local seismic monitoring network and show clear spatial correlation between open-hole intervals of wells and diffuse seismicity within presumably fault-bounded volumes. Schoenball et al. [2015] showed that seismicity in study area B changes its average depth and is shallower after production commenced.

The inferred induced seismicity is confined to study area B (Figure 2) and closely correlates with the extent of mapped faults [e.g., Davatzes and Hickman, 2010] and the wellfield. Furthermore, there is a distinct lack of seismicity immediately outside of the wellfield, suggesting that the seismicity in study area B is the result of perturbations caused by the operation of the geothermal plant. It is therefore plausible to conclude that the vast majority of seismicity recorded since 1987 in study area B is induced by the field operations such as net fluid production from and cold water reinjection into the crystalline rock. A marginal number of natural events are expected to still occur in study area B.

3. Analysis of Scaling Relations

In the remainder of this paper, we treat earthquakes as point processes that are characterized by hypocenter location, time, and magnitude. Under the assumption that seismicity is predominantly induced in study area B and natural in study area A–B during the coproduction period 1987–2013, we will analyze scaling relations of earthquakes separately for study areas A–B and B during the coproduction period. We do not attempt this for the preproduction period 1981–1986 since the data quantity and quality (absolute location accuracy and magnitudes) are not sufficient to resolve between study areas A–B and B.

3.1. Magnitude-Frequency Relation

We use the maximum likelihood method [Aki, 1965; Naylor et al., 2009] to determine the b values of the magnitude-frequency relation separately for study areas A–B and B for the coproduction period 1987–2013. The magnitude of completeness M_c was taken as 1.8. We obtain b values of 1.09 and 1.14 for study areas A–B and B, respectively (Figure 3a). The 95% uncertainties are 0.03 and 0.11, respectively. Hence, the determined b values are the same for both study areas within their uncertainties. The b value for the whole catalog in study area A is 1.10 ± 0.03 , which is the same as for study area A–B only. The preproduction b value for study area A is 1.24 ± 0.15 and hence not significantly different from either of the coproduction values. The resulting b values are slightly higher than the average for southern California [Hutton et al., 2010], consistent with the frequent observation of higher b values in volcanic areas [Wiemer et al., 1998; Wyss et al., 2001].

3.2. Correlation Dimension

The spatial distribution of events can be quantified using the spatial correlation dimension d as defined by Grassberger and Procaccia [1983] using the spatial correlation integral:

$$C(r) = \frac{2}{N(N-1)} N(r_0 < r), \quad (1)$$

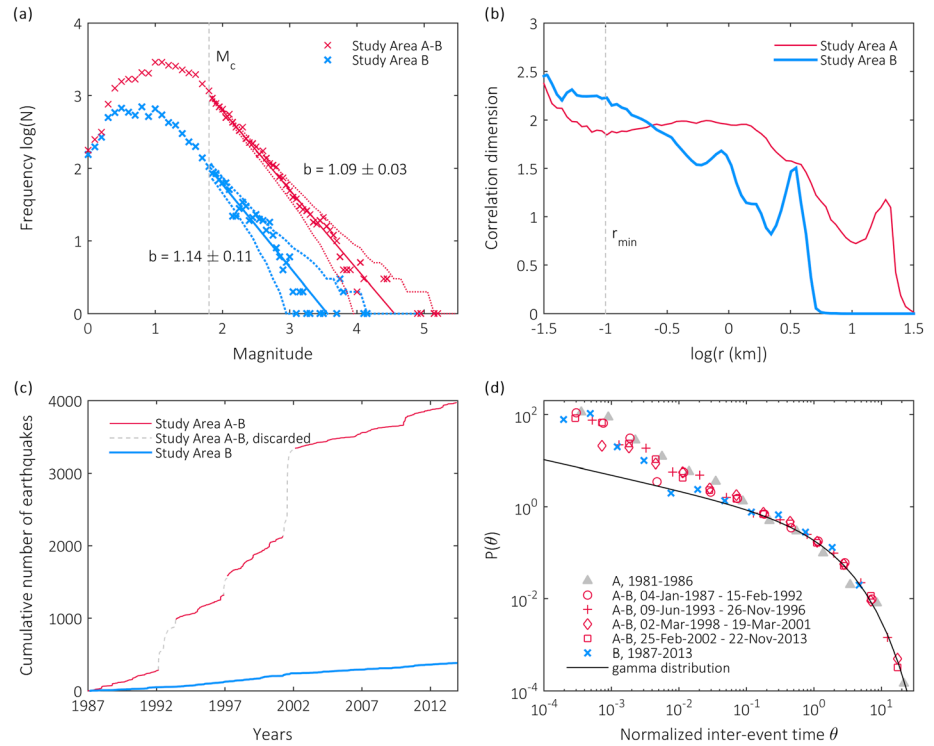


Figure 3. (a) Magnitude-frequency distributions with maximum likelihood estimates of b for both study areas in 1987–2013 and 95% confidence intervals (dotted). (b) Correlation dimension defined as the slope of the correlation integral (equation (1)) as function of interevent distance r for study areas A and B. (c) Cumulative number of earthquakes with $M > M_c$ as a function of time for both study areas. The masked periods were discarded for further analysis of interevent times as described in the text. (d) Probability density function of the time intervals between successive events for the different periods in study area A and for the entire produced period 1987–2013 in study area B.

where N is the total number of events and $N(r_0 < r)$ is the number of events with interevent distances smaller than r . This integral usually follows a power law with the correlation dimension d such that $C(r) \propto r^d$. The log-linear part of the correlation integral used to infer d is limited on the lower end by the location uncertainty of the earthquake catalog [Kagan, 2007]. The r_{\min} should be taken as not smaller than 5 times the location uncertainty. The upper limit r_{\max} is less well defined and is related to the lateral dimensions of the catalog and the distribution of seismicity within the bounding box [Kagan, 2007]. If the correlation dimension d reaches a stable plateau value between r_{\min} and r_{\max} , a meaningful value for d can be derived. For study area A, a plateau with almost constant d is found for $0.1 < r < 1$ km yielding $d \approx 1.8$ (Figure 3b). For study area B it is trickier to find a plateau since the overall extent of the area limits the useful range. For smaller $r < 0.3$ km we find $d > 1.8$ and smaller values for larger r . No significant difference between the correlation dimensions for study areas A and B can be established (Figure 3b). Overall, these results are in agreement with d for southern California as determined by Kagan [2007]. As we highlight below, our analysis is not critically dependent on the quality of determining d .

3.3. Interevent Time

The probabilities of interevent times was proposed to follow a universal distribution for a wide range of data sets for quasistationary periods if time is rescaled with seismicity rate [Corral, 2004]. For catalogs with an average seismicity rate $1/\langle\tau\rangle$ and interevent time τ the probability densities of interevent times $P(\theta)$ with $\theta = \tau/\langle\tau\rangle$ follow a gamma distribution as

$$P(\theta) = \frac{C}{\langle\tau\rangle\theta^{1-\gamma}} \exp\left(-\frac{\theta}{B}\right), \quad (2)$$

with parameters C , γ , and B . Studying arbitrary periods, Molchan [2005] and Hainzl et al. [2006] showed that B represents the fraction of background events and that there is no universal distribution of interevent times.

Following *Corral* [2004] we create time bins that are equally sized in logarithmic time and count the number of consecutive event pairs with interevent times that fall into these bins and divide the counts by the total number of events in the catalog and by the size of the bins. We apply this method on the complete part of the catalog, i.e., for events with $M > M_c$ of 1.8 and individually for study areas A–B and B. Since the number of earthquakes in study area A–B is dominated by few major mainshock-aftershock sequences and swarms (Figure 3c), we remove these periods of abnormal activity and use the individual periods of about constant seismicity rate to compute the probability densities. This procedure was proposed by *Corral* [2004] who removed episodes with major earthquake sequences where the earthquake rate is far from stationary and the proportion of background to clustered events varies strongly [*Molchan*, 2005].

We obtain a very good fit of $P(\theta)$ for all periods in study area A–B and the entire period in study area B with the gamma distribution and the parameters determined by *Corral* [2004] for global seismicity ($\gamma = 0.67$, $C = 0.5$ and $B = 1.58$) (Figure 3d). We cannot find a significant variation of the distribution of interevent times between study areas A–B and B. Our results obtained here are in agreement with previous studies on mining-induced and injection-induced seismicity that behave in the same fashion as tectonic earthquakes [*Davidson et al.*, 2013].

3.4. Space-Time-Magnitude Statistics

So far we have shown that seismicity around the geothermal field (study areas A–B) and seismicity in the geothermal field (study area B) have indistinguishable statistical properties of their magnitude-frequency relation, their spatial distribution, and their interevent times. In the next section we use all components of the earthquake point process vector (location, time, and magnitude) to identify clear differences between the study areas that begin with the onset of production in 1987.

We compute nearest neighbor distances in the space-time-magnitude domain [*Baiesi and Paczuski*, 2004] for each pair of events i and j using

$$\eta_{ij} = \begin{cases} t_{ij} (r_{ij})^d 10^{-bm_i}, & t_{ij} > 0 \\ \infty, & t_{ij} < 0 \end{cases}, \quad (3)$$

where $t_{ij} = t_j - t_i$ is the interevent time, r_{ij} is the interevent distance in Euclidean space, and the b value of the magnitude frequency relation and magnitude m_i of event i . The parameters $b = 1.11$ and $d = 1.8$ were determined as described above. As shown, they are indistinguishable for study areas A–B and B and hence are treated as constant over study area A.

Histograms of η for all earthquakes in a catalog typically show two modes: a mode of background seismicity at large values of η and a mode of clustered seismicity for small values of η [*Zaliapin et al.*, 2008]. Following *Zaliapin et al.* [2008], we can decompose the interevent distance η (equation (1)) into a rescaled distance R and a rescaled time T :

$$R_{ij} = (r_{ij})^d 10^{-bm_i/2}, \quad (4)$$

$$T_{ij} = t_{ij} 10^{-bm_i/2} \quad (5)$$

with

$$\eta_{ij} = R_{ij} T_{ij}. \quad (6)$$

We continue by computing a histogram of the nearest neighbor distance η and plot it in the T-R domain. We do this separately for study areas A–B and B and for different time windows. We chose a time interval of 6.6 years which divides the whole study period of 1981–2013 into five equal time windows with the first time window from 1981 to mid-1987 being the preproduction period. Nevertheless, the nearest neighbor for each event was still determined among events of the whole catalog period since 1981 preceding that event. The binning into time windows has no effect on the computation of η . The histograms were strongly influenced by the July 2001 swarm and its M5.1 mainshock. For a large number of subsequent events the M5.1 mainshock is their nearest neighbor based on η which distorts the T-R histograms (Figure S4). Therefore, to compute the histograms, we removed all events that have the M5.1 event as their nearest neighbor (Figure 4).

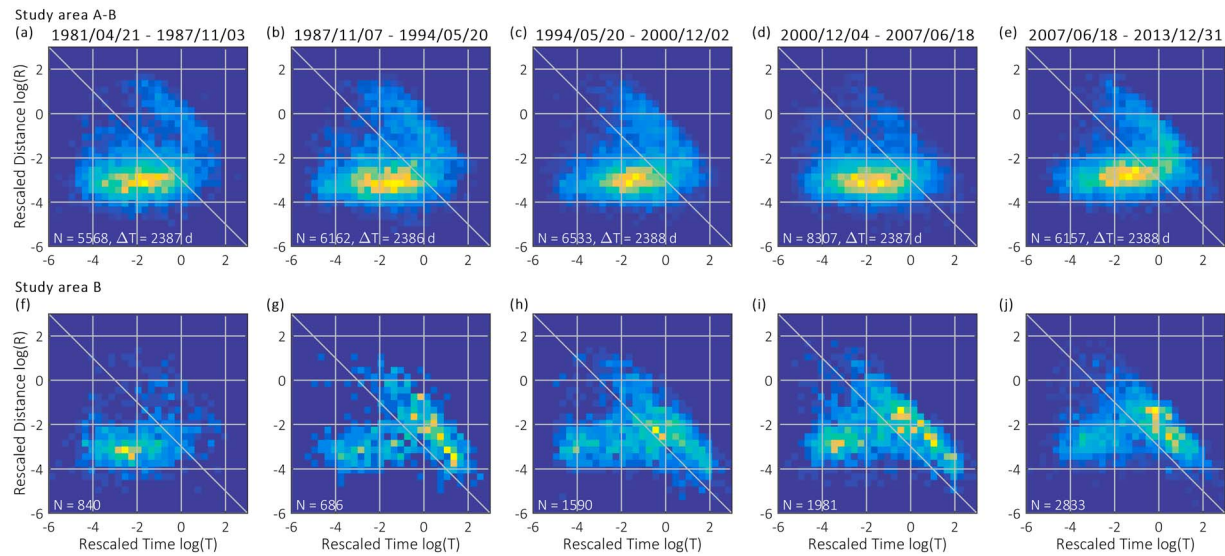


Figure 4. T-R histograms for study areas (top row) A–B and (bottom row) B for different time periods of the same length. The first time interval is mostly preproduction, whereas the later intervals are coproduction. The color scale is normalized for each plot.

Generally all histograms feature two modes that are separated by a diagonal given by $\log_{10}(T/R) \approx -3$. The mode above the diagonal represents the Poissonian background seismicity along a diagonal with $T \times R = \text{constant}$, whereas the mode below the diagonal that forms an elliptical patch along $R = \text{constant}$ represents clustered seismicity relatively close in time and space [Zaliapin *et al.*, 2008; Zaliapin and Ben-Zion, 2013]. The coproduction intervals of study area B (Figures 4g–4j) have background modes that extend by about 1 order of magnitude further along the diagonal to larger T and accordingly smaller R compared to the histograms for study area A–B for all time intervals and also the preproduction time interval of study area B (Figures 4a–4f). This new population of earthquake pairs among the induced seismicity is observed consistently over all coproduction time intervals and appears to be stable for all four coproduction intervals. It is absent in any of the space-time bins where only natural seismicity is expected. Furthermore, we observe that the intensities of the background versus the cluster modes, i.e., the fraction of background events, increases considerably for all four coproduction intervals in study area B.

4. Discussion

We computed the T-R histograms using the catalog regardless of M_c , and thus, an incomplete catalog that might introduce artifacts. We study the possible bias by introducing a cutoff magnitude for the computation of nearest neighbors and their distribution in T-R space (Figure S5). We find that the distributions are stable regardless of the cutoff magnitude. Specifically, the population at large T and small R and the increased fraction of background events for study area B persist. This observation is in line with results by Gu *et al.* [2013]. We estimated μ , the fraction of events in the background mode from the distribution of nearest neighbors in T-R space by fitting a 2-D Gaussian mixture model to the distribution obtained for the complete part of the catalog of the coproduction period. The fraction of background events is then obtained from the relative intensities of the two Gaussian modes (Figure S6). Using all events with $M \geq M_c$ during 1987–2013, this yields $\mu = 0.22$ for study area A–B and $\mu = 0.81$ for study area B. Another method solely based on the interevent time distribution was proposed by Hainzl *et al.* [2006]. This method assumes that background events are Poissonian distributed and may trigger Omori-type aftershock sequences leading to a distribution of interevent times following the gamma distribution (2). We obtain $\mu = 0.17$ for study area A–B and $\mu = 0.44$ for study area B. While there is considerable disagreement between the two methods to determine μ , they do agree on a considerably larger background fraction for study area B. The differences are within the uncertainty expected for this kind of analysis [Hainzl *et al.*, 2006] and probably arise due to the nonstationarity of the background rate, leading to a higher variance of interevent times and an underestimation of the background fraction by the method of Hainzl *et al.* [2006].

The two modes of seismicity are overlapping and a perfect separation is not possible. For higher background seismicity rates in a region the background mode is shifted towards the cluster mode and smaller values of η (see also Figure S5). Thus, the value of η_0 that differentiates clustered from background seismicity decreases as the seismicity rate per area increases. This effect is evident in Figures 4a–4f where the background mode in the preproduction period of study area B or in study area A–B lies well above the diagonal, whereas the coproduction background mode of study area B (featuring a high seismicity rate per area) is just above the diagonal. The background rate, or inversely the magnitude of completeness, has no pronounced effect on the extent of the background mode along the $\eta = \text{constant}$ diagonal (Figure S5).

The stability of the nearest neighbor identification under variation of b and d parameters was analyzed in detail by Zaliapin and Ben-Zion [2013]. They find a negligible influence on the performance due to variation of d within 0.5 units from the true value. Varying b within its 95% confidence range ($0.95 < b < 1.27$) and ($1.3 < d < 2.3$) does not affect the distributions of η in T-R space significantly and the earthquake population at large T ; small R persists to stand out for the coproduction period in study area B. Further analysis of these event pairs shows their interevent distance r_{ij} to cluster around 30 m with interevent times r_{ij} on the order of months to years (Figure S7). The interevent distances are at the limit of the catalog resolutions and might be even below that. We interpret these event pairs as slippage of neighboring asperities on previously active faults after time spans long enough to reload these faults by the various loading mechanisms accompanying geothermal power production.

Previous analyses of seismicity induced during stimulation of enhanced geothermal systems have shown that induced seismicity mostly appears as Poissonian background seismicity [Langenbruch *et al.*, 2011]. This is consistent with the rate-and-state formulation of background rate being proportional to stressing rate [Dieterich, 1994] promoted through pore pressure increase [Hakimhashemi *et al.*, 2014]. Also no substantial triggering effect by static stress transfer could be inferred [Schoenball *et al.*, 2012] leading to the conclusion that induced seismicity mostly behaves as independent background events albeit at a higher activity level. Although we did not show here that there are repeating earthquakes on collocated asperities, this has been observed at several geothermal production sites that penetrate basement rock [Bourouis and Bernard, 2007; Deichmann *et al.*, 2014; Lengliné *et al.*, 2014] and might also be the case at Coso [Lees, 1998].

5. Conclusions

The comparative analysis of natural and induced seismicity at the same tectonic setting at the CGF revealed no significant differences of the frequency-size distribution and of interevent times. The spatial dimension of seismicity in the study area does not provide conclusive evidence for a distinction between both types of seismicity either. Instead, we analyzed distributions of the nearest neighbor distance derived from a space-time-magnitude metric. Induced earthquakes occur predominantly as background seismicity and feature a population of earthquake pairs with particularly large rescaled interevent time and small rescaled distance. Unlike tectonic processes, stress changes by the field operations occur on much smaller time scale and appear strong enough to drive small scale faults through several seismic cycles. As a result, we record seismicity close to previous hypocenters after a time period on the order of a year. While few similar earthquake pairs exist in the tectonic dominated study area A–B, they are much more abundant and are a distinctive feature of induced seismicity in study area B.

References

- Aki, K. (1965), Maximum likelihood estimate of b in the formula $\log N = a - bM$ and its confidence limits, *Bull. Earthquake Res. Inst.*, *43*, 237–239.
- Baiesi, M., and M. Paczuski (2004), Scale-free networks of earthquakes and aftershocks, *Phys. Rev. E*, *69*, 066106, doi:10.1103/PhysRevE.69.066106.
- Ben-Zion, Y. (2008), Collective behavior of earthquakes and faults: Continuum-discrete transitions, progressive evolutionary changes, and different dynamic regimes, *Rev. Geophys.*, *46*, RG4006, doi:10.1029/2008RG000260.
- Bourouis, S., and P. Bernard (2007), Evidence for coupled seismic and aseismic fault slip during water injection in the geothermal site of Soultz (France), and implications for seismogenic transients, *Geophys. J. Int.*, *169*(2), 723–732, doi:10.1111/j.1365-246X.2006.03325.x.
- Combs, J., and Y. Rotstein (1975), Microearthquake studies at the Coso geothermal area, China Lake, California, in *Proceedings of the 2nd U.N. Symposium on the Development and Use of Geothermal Resources*, pp. 909–916, San Francisco, Calif. [Available at catalog.hathitrust.org/Record/000128507.]
- Corral, Á. (2004), Long-term clustering, scaling, and universality in the temporal occurrence of earthquakes, *Phys. Rev. Lett.*, *92*(10), 108501, doi:10.1103/PhysRevLett.92.108501.

Acknowledgments

Injection and production data are taken from the DOGGR database of the California Department of Conservation (<http://www.conservation.ca.gov/dog>). The relocated catalog for southern California for 1981–2013 is available from the SCEDC website (<http://scedc.caltech.edu/research-tools/alt-2011-dd-hauksson-yang-shearer.html>). Navy GPO and Terra-Gen provided well trajectory data. This work is supported by Temple University and the U.S. Geological Survey's (USGS) Energy Program's Geothermal Project. M. Schoenball is financed by Cooperative Agreement Number G13AC00283 from the USGS to Temple University: Geothermal Systems in the Western U.S. We acknowledge reviews by Andrea Llenos, Jeanne Hardebeck, Art McGarr, and an anonymous reviewer that considerably helped to improve the manuscript. Any use of trade, firm, or product names is for descriptive purposes only and does not imply endorsement by the U.S. Government.

The Editor thanks Art McGarr and an anonymous reviewer for their assistance in evaluating this paper.

- Davatzes, N. C., and S. H. Hickman (2010), The feedback between stress, faulting, and fluid flow: Lessons from the Coso Geothermal Field, CA, USA, in *World Geothermal Congress*, p. 15, Int. Geotherm. Assoc., Bali, Indonesia, 25–29 April.
- Davidson, J., G. Kwiatek, and G. Dresen (2013), Earthquake interevent time distribution for induced micro-, nano-, and picoseismicity, *Phys. Rev. Lett.*, *110*(6), 068501, doi:10.1103/PhysRevLett.110.068501.
- Deichmann, N., T. Kraft, and K. F. Evans (2014), Identification of faults activated during the stimulation of the Basel geothermal project from cluster analysis and focal mechanisms of the larger magnitude events, *Geothermics*, *52*, 84–97, doi:10.1016/j.geothermics.2014.04.001.
- Dieterich, J. H. (1994), A constitutive law for rate of earthquake production and its application to earthquake clustering, *J. Geophys. Res.*, *99*(B2), 2601–2618, doi:10.1029/93JB02581.
- Ellsworth, W. L. (2013), Injection-induced earthquakes, *Science*, *341*, doi:10.1126/science.1225942.
- Feng, Q., and J. M. Lees (1998), Microseismicity, stress, and fracture in the Coso geothermal field, California, *Tectonophysics*, *289*(1–3), 221–238, doi:10.1016/S0040-1951(97)00317-X.
- Fialko, Y., and M. Simons (2000), Deformation and seismicity in the Coso geothermal area, Inyo County, California: Observations and modeling using satellite radar interferometry, *J. Geophys. Res.*, *105*(B9), 21,781–21,793, doi:10.1029/2000JB900169.
- Grassberger, P., and I. Procaccia (1983), Measuring the strangeness of strange attractors, *Phys. D Nonlinear Phenom.*, *9*(1–2), 189–208, doi:10.1016/0167-2789(83)90298-1.
- Grünthal, G. (2014), Induced seismicity related to geothermal projects versus natural tectonic earthquakes and other types of induced seismic events in Central Europe, *Geothermics*, *52*, 22–35, doi:10.1016/j.geothermics.2013.09.009.
- Gu, C., A. Y. Schumann, M. Baiesi, and J. Davidson (2013), Triggering cascades and statistical properties of aftershocks, *J. Geophys. Res. Solid Earth*, *118*, 4278–4295, doi:10.1002/jgrb.50306.
- Hainzl, S., F. Scherbaum, and C. Beauval (2006), Estimating background activity based on interevent-time distribution, *Bull. Seismol. Soc. Am.*, *96*(1), 313–320, doi:10.1785/0120050053.
- Hakimshemi, A. H., M. Schoenball, O. Heidebach, A. Zang, and G. Grünthal (2014), Forward modelling of seismicity rate changes in georeservoirs with a hybrid geomechanical-statistical prototype model, *Geothermics*, *52*, 185–194, doi:10.1016/j.geothermics.2014.01.001.
- Hauksson, E., and J. Unruh (2007), Regional tectonics of the Coso geothermal area along the intracontinental plate boundary in central eastern California: Three-dimensional Vp and Vp/Vs models, spatial-temporal seismicity patterns, and seismogenic deformation, *J. Geophys. Res.*, *112*, B06309, doi:10.1029/2006JB004721.
- Hauksson, E., W. Yang, and P. M. Shearer (2012), Waveform relocated earthquake catalog for southern California (1981 to June 2011), *Bull. Seismol. Soc. Am.*, *102*(5), 2239–2244, doi:10.1785/0120120010.
- Hutton, K., J. Woessner, and E. Hauksson (2010), Earthquake monitoring in southern California for seventy-seven years (1932–2008), *Bull. Seismol. Soc. Am.*, *100*(2), 423–446, doi:10.1785/0120090130.
- Julian, B. R., G. R. Foulger, F. C. Monastero, and S. Bjornstad (2010), Imaging hydraulic fractures in a geothermal reservoir, *Geophys. Res. Lett.*, *37*, L07305, doi:10.1029/2009GL040933.
- Kagan, Y. Y. (2007), Earthquake spatial distribution: The correlation dimension, *Geophys. J. Int.*, *168*(3), 1175–1194, doi:10.1111/j.1365-246X.2006.03251.x.
- Kanamori, H., and E. E. Brodsky (2004), The physics of earthquakes, *Rep. Prog. Phys.*, *67*(8), 1429–1496, doi:10.1088/0034-4885/67/8/R03.
- Kaven, J. O., S. H. Hickman, and N. C. Davatzes (2014), Micro-seismicity and seismic moment release within the Coso Geothermal Field, California, in *Stanford Geothermal Workshop, Proceedings, 39th Workshop on Geothermal Reservoir Engineering*, p. 10, Stanford Univ., Stanford, Calif.
- Langenbruch, C., C. Dinske, and S. A. Shapiro (2011), Inter event times of fluid induced earthquakes suggest their Poisson nature, *Geophys. Res. Lett.*, *38*, L21302, doi:10.1029/2011GL049474.
- Lees, J. M. (1998), Multiplet analysis at Coso geothermal, *Bull. Seismol. Soc. Am.*, *88*(5), 1127–1143.
- Lengliné, O., L. Lamourette, L. Vivin, N. Cuenot, and J. Schmittbuhl (2014), Fluid-induced earthquakes with variable stress drop, *J. Geophys. Res. Solid Earth*, *119*, 8900–8913, doi:10.1002/2014JB011282.
- Malin, P. E. (1994), The seismology of extensional hydrothermal systems, *GRC Trans.*, *18*, 17–22.
- Manley, C. R., and C. R. Bacon (2000), Rhyolite thermobarometry and the shallowing of the magma reservoir, Coso volcanic field, California, *J. Petrol.*, *41*(1), 149–174, doi:10.1093/petrology/41.1.149.
- Molchan, G. (2005), Interevent time distribution in seismicity: A theoretical approach, *Pure Appl. Geophys.*, *162*(6–7), 1135–1150, doi:10.1007/s00024-004-2664-5.
- Monastero, F. C. (2002), Model for success, *GRC Bull.*, 188–194.
- Naylor, M., J. Greenhough, J. McCloskey, A. F. Bell, and I. G. Main (2009), Statistical evaluation of characteristic earthquakes in the frequency-magnitude distributions of Sumatra and other subduction zone regions, *Geophys. Res. Lett.*, *36*, L20303, doi:10.1029/2009GL040460.
- Schoenball, M., C. Baujard, T. Kohl, and L. Dorbath (2012), The role of triggering by static stress transfer during geothermal reservoir stimulation, *J. Geophys. Res.*, *117* B09307, doi:10.1029/2012JB009304.
- Schoenball, M., J. O. Kaven, J. M. G. Glen, and N. C. Davatzes (2015), Natural or induced: Identifying natural and induced swarms from pre-production and co-production microseismic catalogs at the Coso Geothermal Field, in *40th Workshop on Geothermal Reservoir Engineering*, p. 11, Curran Assoc., Red Hook, N. Y.
- Walter, A. W., and C. S. Weaver (1980), Seismicity of the Coso Range, California, *J. Geophys. Res.*, *85*(B5), 2441–2458, doi:10.1029/JB085iB05p02441.
- Wiemer, S., S. R. McNutt, and M. Wyss (1998), Temporal and three-dimensional spatial analyses of the frequency-magnitude distribution near Long Valley Caldera, California, *Geophys. J. Int.*, *134*(2), 409–421, doi:10.1046/j.1365-246X.1998.00561.x.
- Woessner, J., and S. Wiemer (2005), Assessing the quality of earthquake catalogues: Estimating the magnitude of completeness and its uncertainty, *Bull. Seismol. Soc. Am.*, *95*(2), 684–698, doi:10.1785/0120040007.
- Wyss, M., F. Klein, K. Nagamine, and S. Wiemer (2001), Anomalously high b-values in the South Flank of Kilauea volcano, Hawaii: Evidence for the distribution of magma below Kilauea's East rift zone, *J. Volcanol. Geotherm. Res.*, *106*(1–2), 23–37, doi:10.1016/S0377-0273(00)00263-8.
- Zaliapin, I., and Y. Ben-Zion (2013), Earthquake clusters in southern California I: Identification and stability, *J. Geophys. Res. Solid Earth*, *118*, 2847–2864, doi:10.1002/jgrb.50179.
- Zaliapin, I., A. Gabrieli, V. Keilis-Borok, and H. Wong (2008), Clustering analysis of seismicity and aftershock identification, *Phys. Rev. Lett.*, *101*, 018501, doi:10.1103/PhysRevLett.101.018501.
- Zang, A., V. Oye, P. Jousset, N. Deichmann, R. Gritto, A. McGarr, E. Majer, and D. Bruhn (2014), Analysis of induced seismicity in geothermal reservoirs – An overview, *Geothermics*, *52*, 6–21, doi:10.1016/j.geothermics.2014.06.005.